On the (de)stabilization of draw resonance due to cooling

BENOIT SCHEID[1], SARA QUILIGOTTI[2], BINH TRAN[2], RENÉ GY[2] AND HOWARD A. STONE[1]

[1]School of Engineering and Applied Sciences, Harvard University, Cambridge, MA 02138, USA
[2]Saint-Gobain Recherche, 39 Quai Lucien Lefranc, B.P. 135, 93303 Aubervilliers Cedex, France

We study the drawing of a Newtonian viscous sheet under the influence of cooling with temperature dependence of the viscosity. Classically this problem has an instability called draw resonance, when the draw ratio Dr, which is the ratio of the outlet velocity relative to the inlet velocity, is beyond a critical value Dr_c. The heat transfer from the surface compared to the bulk energy advection is conveniently measured by the Stanton number St. Usual descriptions of the problem are one-dimensional and rigorously apply for $St \leq 1$. The model presented here accounts for variations of the temperature across the sheet and has therefore no restriction on St. Stability analysis of the model shows two different cooling regimes: the 'advection-dominated' cooling for $St \ll 1$ and the 'transfer-dominated' cooling for $St \gg 1$. The transition between those two regimes occurs at $St = O(1)$ where the stabilizing effect due to cooling is most efficient, and for which we propose a mechanism for stabilization, based on phase shifts between the tension and axial-averaged flow quantities. Away from this transition, the sheet is shown to always be unstable at smaller draw ratios. Additionally, in the limit of $St \to \infty$, the heat exchange is such that the temperature of the fluid obtains the far-field temperature, which hence corresponds to a 'prescribed temperature' regime. This dynamical situation is comparable to the isothermal regime in the sense the temperature perturbation has no effect on the stability properties. Nevertheless, in this regime, the critical draw ratio for draw resonance can be below the classical value of $Dr_c = 20.218$ obtained in isothermal conditions.

1. Introduction

Drawing or stretching viscous sheets are encountered in the polymer film industry, e.g. the film casting process, as well as in the glass sheet industry. The basic fluid mechanical problem is sketched in figure 1, which shows the thinning of a sheet. Sheet stretching encountered in film casting processes shares many similarities with thread drawing encountered in fiber spinning processes. Both fiber spinning and film casting processes have been extensively studied in the literature (see e.g. Pearson (1985)). One of the similarities is the short residence time ($\sim 10 \, \text{sec.}$) of the fluid between the inlet and the take-up. On the contrary, typical fluid residence time in glass sheet processes are much longer ($\sim 10 \, \text{min.}$), which may significantly modify the heat exchanges between the fluid and its surrounding, and through temperature dependence of the viscosity, modify the hydrodynamic behavior and consequently the stability properties for the so-called draw resonance phenomenon.

Draw resonance is a well-known instability that occurs for stretching viscous sheets

(respectively, threads), which is characterized by oscillatory variations in thickness (respectively, diameter). The principal control parameter is the draw ratio Dr, namely the take-up speed relative to the speed at the inlet; the stretching process is unstable for $Dr > Dr_c$. In fact, the spatially uniform but time-dependent tension provides a natural feedback mechanism between the exit and the inlet, which sustains oscillations above the critical draw ratio Dr_c.

In isothermal conditions, $Dr_c = 20.218$ for both threads and sheets. However, in industrial processes, fibers can be stably drawn at very high speeds, e.g. $Dr = O(10^5)$. Shah & Pearson (1972a) found that convective heat transfer is responsible for such a strong stabilization. However, as shown by these authors and subsequent works (see e.g. Gupta *et al.* (1996)), regimes in fiber spinning intrinsically correspond to small Stanton numbers ($St \leq 1$) — the Stanton number is the ratio of the surface heat transfer relative to the bulk energy advection. In contrast, sheet stretching processes can in certain circumstances correspond to large Stanton numbers ($St \gg 1$). Again from the fiber spinning literature, Fisher & Denn (1977) have shown that though the cooling by convective heat transfer has a stabilizing effect for small Stanton numbers, there should be a reverse trend toward large Stanton numbers. Indeed, the limit $St \rightarrow \infty$ means the liquid has obtained the ambient temperature and is effectively in isothermal conditions. However, this is rigorously true if (i) the ambient temperature is constant, which is never the case in practice, (ii) the one-dimensional assumption is applicable (i.e. no radial temperature variations), which strictly forbids the study of large Stanton number ($St \gg 1$) regimes. We also mention that Geyling & Homsy (1980) and Willien *et al.* (1988) have shown for glass fibers that though pure convective heat transfer is always stabilizing, adding radiative heat transfer can be destabilizing for sufficiently large values of the radiative heat transfer coefficient. This result indicates the non-monotonic behavior of the neutral stability for increasing Stanton number when it depends on both convective and radiative heat transfer coefficients.

Despite the extended literature for the stability of fiber spinning in non-isothermal conditions, to our knowledge, the stability of film casting in non-isothermal conditions has only been treated by Minoshima & White (1983) in the limit of small St. Here we aim to explore the entire range of St. Moreover, though the one-dimensional stress and continuity equations describing the evolution of the cross-sectional area are identical for fibers and films (Yeow 1974), the similarity does not hold for the energy equation†. As a consequence, stability results obtained for non-isothermal fiber drawing are not applicable to the stability of non-isothermal film drawing, *i.e* the critical draw ratios are not comparable. While most works on draw resonance focus on cooling for practical reasons, Wylie *et al.* (2007) have recently investigated heating during thread drawing. They found that steady-state solutions are not unique — *i.e.* several possible states exist for a certain draw ratio — if the viscosity varies sufficiently abruptly with temperature and heating is strong enough to cause sufficiently large variations. In these specific conditions, they found 'thermal' instabilities (both oscillatory and non-oscillatory) that occur in small isolated windows of the draw ratio. However, as far as it has been explored so far and as shown in this paper, no multiple solutions or new types of instability other than draw resonance has ever been observed under cooling conditions for threads or for film drawing; nevertheless, cooling can significantly alter the threshold and frequency of draw resonance.

In numerical simulations for non-isothermal film casting processes, efforts have been

---

† There is a square root of the cross-sectional area that appears in the denominator of the transverse heat diffusion term in the one-dimensional heat equation for fibers and not for films.

focused on studying the influence of non-isothermal conditions on the neck-in and edge bead defects in steady-state conditions and for polymer melts; *e.g.* Sollogoub *et al.* (2006) used a two-dimensional model and Zheng *et al.* (2006) used a three-dimensional description. In both cases, it is shown that the effect of viscoelasticity and heat transfer coefficient are similar, which is to concentrate the film stretching in the flow area near the inlet. This observation is also made in the present paper, which is a consequence of the abrupt variation of the viscosity with temperature. Shin *et al.* (2007) additionally performed time-dependent simulations using a two-dimensional model and showed transient solutions of the dynamics in non-isothermal polymer film casting. They found that both the amplitude and period of oscillations for draw resonance are in good agreement with available experimental data.

In this paper we investigate the stretching of a Newtonian liquid film using a one-dimensional model that aims to explore the entire range of Stanton numbers by allowing the temperature to vary across the thickness of the film. Because convective/radiative heat transfer characteristics can strongly differ depending on practical applications and because they are rarely known with sufficient accuracy, we have chosen to use the Newton's cooling law with a constant heat transfer coefficient. Also we allow the ambient temperature to vary along the stretching direction. Though more arbitrary and simpler than in practical applications, prescribing the ambient temperature distribution along the stretching direction is the same (when multiplied by the constant heat transfer coefficient) as imposing a heat flux distribution, which thus mimics realistic operating conditions.

We also model the transition to a solid by increasing the viscosity to a large value as the temperature approaches the transition temperature. Though this approach ignores details of solidification such as anisotropy depending on the processing conditions in the case of polymer crystallization (see *e.g.* Barot & Rao (2004) for details), this approach is expected to be satisfactory in accounting for glass transition. In any case, assuming that heat released during solidification can be ignored is valid because the glass transition occurs at take-up, after the geometry is no longer changing (see *e.g.* Smith & Stolle (2000)). In the case of glass fibers, Forest *et al.* (2000) have considered a more general two-phase model with a solidification front at the transition temperature. They nevertheless reached the conclusion that a 'one-phase' model has the crucial advantage that solutions have continuous gradients at the glass transition free boundary, which not only is consistent with experiments but further enables one to perform a linear stability analysis of these steady boundary-value states; it is a 'one-phase' approach that we thus adopt herein.

In draw resonance, and because of the nature of the equations, none of the dependent variables are in phase with each other, at any position from the inlet to the take-up, which challenges both intuition and understanding of the basic mechanisms underlying the instability. In isothermal conditions and for Newtonian fluids, Hyun (1978) proposed an approximate criterion for the occurrence of draw resonance based on the fact that the mass of fluid that enters the system at a constant rate must leave the system in a fixed amount in every cycle of draw resonance. Kim *et al.* (1996) later refined Hyun's criterion by using kinematic wave theory. They showed that draw resonance can occur only if the time $(2t_L)$ needed for two successive unity-throughput waves augmented by half a period of oscillation (P) is equal or smaller than the traveling time (2ϑ) for two successive extremum-thickness waves† to cover the entire length of the system. In mathematical

---

† The time ϑ_L is the time that takes either the maximum or the minimum of a 'resonant' thickness perturbation to propagate from the inlet to the take-up position.
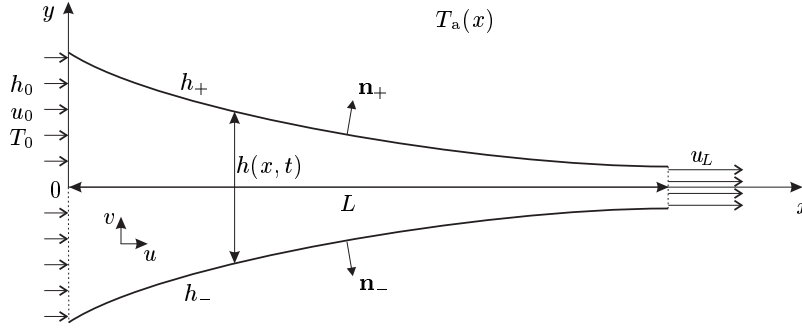
FIGURE 1. Stretching viscous sheet.

terms, this criterion has the form

$$2t_L + \frac{P}{2} \le 2\vartheta_L \qquad \text{for} \qquad Dr \ge Dr_{\mathrm{c}} \,. \tag{1.1}$$

Jung, Hyun and coworkers have furthermore demonstrated that (1.1) also applies for viscoelastic fluids, using both nonlinear simulations (Jung *et al.* 2000) and linear theory (Lee *et al.* 2005). These results suggest universality of the criterion by Kim *et al.* (1996), which should thus also apply for non-isothermal draw resonance, as we will explore in this paper, along with the mechanism responsible for the stabilization of draw resonance due to cooling. Indeed, despite the extended number of works on draw resonance in non-isothermal conditions, to our knowledge, none of them have explicitly addressed the physical mechanism responsible for such a stabilization. Some elements of an answer can be found in Jung *et al.* (1999) who showed through dedicated numerical simulations that the sensitivity of the axial tension to disturbances decreases as the cooling increases, which is a response in favor of stability. Using insights from the vast research of the 'Korean school' on draw resonance, spread over the last three decades — research mainly based on nonlinear simulations with the exception of Lee *et al.* (2005) — we further elucidate in this paper the stabilizing mechanism due to cooling, using results exclusively obtained from linear stability theory.

The model used in this paper is presented in §2. We then outline the stability calculation in §3 and systematically investigate the influence of heat transfer in §4. We will identify a new regime for high Stanton numbers where the heat transfer to the surroundings can play a destabilizing role. The prescribed temperature regime in the limit of infinite Stanton number is discussed in §5. In §6, we propose a scenario for the stabilizing mechanism of draw resonance due to cooling based on a new idea that involves phase shifts between axial tension and relevant spatially averaged quantities of the system. Finally in §7, we test both the criteria of Hyun (1978) and Kim *et al.* (1996) and show how the different times involved in those criteria are affected by cooling. Concluding remarks are presented in §8.

2. The model

We consider a two-dimensional viscous liquid sheet with thickness h_0, velocity u_0 and temperature T_0 at the inlet being stretched over a length L to the take-up speed u_L, as sketched in figure 1. The draw ratio is denoted $Dr = u_L/u_0$. The sheet has thickness $h(x,t)$ and is assumed to be symmetric around $y = 0$, where the positions of the upper and lower interfaces are denoted $h_\pm \equiv \pm\frac{1}{2}h(x,t)$.

2.1. *The flow field*

The flow field is assumed to be described by the continuity and the Stokes equations,

$$\boldsymbol{\nabla} \cdot \mathbf{u} = 0 \, , \tag{2.1a}$$

$$\boldsymbol{\nabla} \cdot \boldsymbol{\sigma} = \mathbf{0} \, , \tag{2.1b}$$

with the operator $\boldsymbol{\nabla} = (\partial_x, \partial_y)$, the velocity field $\mathbf{u} = (u, v)$, and the Newtonian stress tensor $\sigma_{ij} = -p\delta_{ij} + \eta(\partial_j u_i + \partial_i u_j)$, where p is the pressure and $\eta = \eta(T)$ is the dynamical viscosity with T the temperature. The boundary conditions at the free surfaces $y = h_\pm$, are the kinematic condition and the stress balance,

$$\partial_t h_\pm + u\big|_{h_\pm} \partial_x h_\pm - v\big|_{h_\pm} = 0 \, , \tag{2.2a}$$

$$\mathbf{n}_\pm \cdot \boldsymbol{\sigma}\big|_{h_\pm} = 0 \, , \tag{2.2b}$$

where $\mathbf{n}_\pm = \pm(-\partial_x h_\pm, 1)/n$ is the outward normal vector with $n = \sqrt{1 + \frac{1}{4}(\partial_x h)^2}$. Note the ambient pressure has been taken to be zero for simplicity and the influence of surface tension has been neglected. We follow standard characterizations of thin-films flow (e.g. see Howell (1996)) and for completeness provide the main steps. The above system is made dimensionless through the transformations:

$$x \to Lx, \; y \to \varepsilon Ly, \; h \to \varepsilon Lh, \; t \to \frac{L}{u_0}t, \; u \to u_0 u, \; v \to \varepsilon u_0 v, \; \eta \to \eta_0 \eta, \; p \to \frac{\eta_0 u_0}{L} p, \tag{2.3}$$

where $\varepsilon = h_0/L$ is the *film parameter* and $\eta_0 = \eta(T_0)$, which indicates the average viscosity at the inlet. The dimensionless momentum equations then have the form, with $\sigma_{yx} = \sigma_{xy}$,

$$\varepsilon^2 \partial_x \sigma_{xx} + \partial_y \sigma_{xy}^* = 0 \, , \tag{2.4a}$$

$$\partial_x \sigma_{xy}^* + \partial_y \sigma_{yy} = 0 \, , \tag{2.4b}$$

where the shear stress component becomes

$$\sigma_{xy}^* = \eta \partial_y u + \varepsilon^2 \eta \partial_x v \, . \tag{2.5}$$

The dimensionless tangential and normal stress conditions at the interfaces are, respectively,

$$\sigma_{xy}^*\big|_{h_\pm} \left(1 - \varepsilon^2 (\partial_x h_\pm)^2\right) + \varepsilon^2 \left(\sigma_{yy}\big|_{h_\pm} - \sigma_{xx}\big|_{h_\pm}\right) \partial_x h_\pm = 0 \, , \tag{2.6a}$$

$$\varepsilon^2 \sigma_{xx}\big|_{h_\pm} (\partial_x h_\pm)^2 - 2\sigma_{xy}^*\big|_{h_\pm} \partial_x h_\pm + \sigma_{yy}\big|_{h_\pm} = 0 \, . \tag{2.6b}$$

At this stage, we shall invoke the smallness of the film parameter $\varepsilon \ll 1$ such that ε is used as an ordering parameter. Therefore, at leading order for $\varepsilon^2 \to 0$, (2.4a) and (2.6a) yield

$$\sigma_{xy}^{*(0)} = \eta \partial_y u^{(0)} = 0 \, , \tag{2.7}$$

where superscripts refer to the corresponding order in the ε^2–expansion. Integrating (2.7) once leads to $u^{(0)} = \bar{u}(x, t)$ where $\bar{u}$ is the extensional velocity that remains to be determined. Note the flow is extensional at leading order, whatever the variation of the viscosity across the sheet. Likewise, (2.4b) and (2.6b), using (2.7), yield

$$\sigma_{yy}^{(0)} = -p^{(0)} + 2\eta \partial_y v^{(0)} = 0 \, . \tag{2.8}$$

At leading order, the dimensional transversal stress remains uniform in the viscous sheet and equal to the ambient pressure. This feature is sometimes referred to as the 'membrane

approximation' (Silagy *et al.* 1996). Integrating (2.1*a*) across the thickness, given $v\big|_0 = 0$ by symmetry, leads to

$$v^{(0)} = -y\partial_x \bar{u} \,, \tag{2.9}$$

which substituted in (2.8) yields

$$p^{(0)} = -2\eta\partial_x \bar{u} \,.$$

The leading-order longitudinal stress σ_{xx} can thus be rewritten as

$$\sigma_{xx}^{(0)} = 4\eta\partial_x \bar{u} \,, \tag{2.10}$$

where the factor 4 is referred to as the 'Trouton ratio', namely the extensional viscosity relative to the shear viscosity. The kinematic condition (2.2*a*) together with (2.9) provides the one-dimensional evolution equation for the film thickness,

$$\partial_t h + \partial_x(h\bar{u}) = 0 \,. \tag{2.11}$$

To close the model for h and $\bar{u}$, we must examine the field equations and boundary conditions at the next order in the expansion. The relevant parts of the $O(\varepsilon^2)$ problem are obtained from the longitudinal stress balance (2.4*a*)†,

$$\partial_y \sigma_{xy}^{*(1)} = -\partial_x \sigma_{xx}^{(0)} \,, \tag{2.12}$$

and from the tangential surface stress balance (2.6*a*) with the use of (2.8),

$$\sigma_{xy}^{*(1)}\big|_{h_\pm} = \sigma_{xx}^{(0)}\big|_{h_\pm} \partial_x h_\pm \,. \tag{2.13}$$

The integration of (2.12) between the lower and upper surfaces, using (2.13), then yields

$$\partial_x \left[\int_{h_-}^{h_+} \sigma_{xx}^{(0)} \, \mathrm{d}y \right] = 0 \,, \tag{2.14}$$

which indicates that the depth-averaged tension remains constant along the sheet. An equivalent constant-tension condition has been derived for fibers by Dewynne *et al.* (1992). Substituting (2.10) into (2.14), and integrating with respect to x, we finally get

$$\hat{\eta}h\partial_x \bar{u} = f(t) \,, \tag{2.15}$$

where $\hat{\eta} = (1/h) \int_{h_-}^{h_+} \eta \, \mathrm{d}y$ is the depth-averaged effective viscosity and $f(t)$ the dimensionless tension in the sheet, per unit length in the spanwise direction (the actual tension is obtained by scaling by $4\varepsilon\eta_0 u_0$). Equation (2.15) extends the classical equation for an extensional flow of a Newtonian fluid (e.g. see Pearson (1985)) to the case of in-depth variations of the viscosity, which remains in turn to be determined through the temperature field. The system (2.11, 2.15) for the three unknowns h, $\bar{u}$ and f is solved with the boundary conditions,

$$h(0,t) = 1 \,, \quad \bar{u}(0,t) = 1 \quad \text{and} \quad \bar{u}(1,t) = Dr \,. \tag{2.16}$$

† Consideration of the transverse stress balance (2.4*b*) would lead to the conclusion that the sheet's centerline will remain straight if it is initially straight (Buckmaster *et al.* 1975), at least as far as the stretching is concerned. However, here this result has been a priori accounted through the symmetry condition used to determine v_0.

2.2. *The temperature field*

The temperature field in the sheet is described by the thermal energy equation, which neglecting viscous heating, is

$$\rho c_p \left(\partial_t T + \mathbf{u} \cdot \boldsymbol{\nabla} T \right) = k \boldsymbol{\nabla}^2 T \ , \tag{2.17}$$

where ρ is the fluid density, c_p the specific heat capacity and k the thermal conductivity; we assume these properties to be independent of the temperature. At the free surfaces, we impose the classical Newton's cooling boundary condition,

$$-k \, \mathbf{n}_\pm \cdot \boldsymbol{\nabla} T \big|_{h_\pm} = \alpha \left(T \big|_{h_\pm} - T_{\mathrm{a}}(x) \right) \ , \tag{2.18}$$

where α is the heat transfer coefficient (identical on the two surfaces) and $T_{\mathrm{a}} = T_{\mathrm{a}}(x)$ is the prescribed far-field ambient temperature, which for generality we assume may vary along the sheet. The temperature is non-dimensionalized with the following transformations

$$T \to T_0 \, T \quad \text{and} \quad T_{\mathrm{a}} \to T_0 \, T_{\mathrm{a}} \ . \tag{2.19}$$

Equation (2.17) thus has the dimensionless form

$$\varepsilon Pe \left(\partial_t T + u \partial_x T + v \partial_y T \right) = \varepsilon^2 \partial_{xx} T + \partial_{yy} T \ . \tag{2.20}$$

The Péclet number $Pe = \rho c_p u_0 h_0 / k$ measures the rate of convection of energy $\rho c_p u_0$ in the flow direction relative to the rate of heat conduction k/h_0 in the transverse direction. In turn, the boundary condition (2.18) has the dimensionless form

$$\left(1 + \varepsilon^2 \frac{1}{4} (\partial_x h)^2 \right)^{-1/2} \left(\partial_y T \big|_{h_\pm} - \varepsilon^2 \partial_x h_\pm \ \partial_x T \big|_{h_\pm} \right) = \mp Bi \left(T \big|_{h_\pm} - T_{\mathrm{a}} \right) \ , \tag{2.21}$$

where the Biot number $Bi = \alpha h_0 / k$ describes the rate of heat transport from the liquid to the surroundings. In this study, we shall consider large Péclet numbers such that $\varepsilon Pe = O(1)$. At leading order, i.e. $\varepsilon^2 \to 0$, (2.20) and (2.21) then reduce to

$$\partial_{yy} T^{(0)} = \varepsilon Pe \left(\partial_t T^{(0)} + \bar{u} \, \partial_x T^{(0)} + v^{(0)} \, \partial_y T^{(0)} \right) \ , \tag{2.22a}$$

$$\partial_y T^{(0)} \big|_{h_\pm} = \mp Bi \left(T^{(0)} \big|_{h_\pm} - T_{\mathrm{a}} \right) \ . \tag{2.22b}$$

In order to eliminate the transverse coordinate y in the system above, we assume a parabolic temperature profile that satisfies the boundary conditions (2.22b) and explicitly introduces the average temperature $\theta = \theta(x, t) \equiv (1/h) \int_{h_-}^{h_+} T^{(0)} \, \mathrm{d}y$. Thus we write

$$T^{(0)}(x, y, t) = T_{\mathrm{a}}(x) + \frac{\theta(x, t) - T_{\mathrm{a}}(x)}{1 + \frac{Bi}{6} h(x, t)} \left(1 + Bi \, h(x, t) \left(\frac{1}{4} - \frac{y^2}{h(x, t)^2} \right) \right) \ . \tag{2.23}$$

Substituting (2.9) and (2.23) into (2.22a), and integrating the latter between the lower and upper surfaces yields, using (2.11),

$$\partial_t \theta + \bar{u} \, \partial_x \theta = -St \, \frac{\theta - T_{\mathrm{a}}(x)}{h(1 + \frac{Bi}{6} h)} \ , \tag{2.24}$$

which is to be solved with the boundary condition $\theta(0, t) = 1$. The Stanton number is defined as

$$St = \frac{2 Bi}{\varepsilon Pe} = \frac{2 \alpha L}{\rho c_p u_0 h_0} \ , \tag{2.25}$$

and compares the actual heat transfer across both interfaces to the energy advected by the main flow.

In the limit of $St \to 0$, the sheet retains all of its thermal energy along the stretching direction and the average temperature remains constant everywhere, i.e. $\theta = 1$. This situation occurs for two particular cases: (i) $Pe \to \infty$ which is the case of a poorly conducting fluid and/or relatively fast speeds, though $T^{(0)}$ can still depend on y for finite Bi; (ii) $Bi \to 0$ in the case of no heat loss at the interfaces, i.e. $T^{(0)} = 1$ everywhere. In contrast, the limit $St \to \infty$, when Bi remains finite, means that the typical speed is slow enough and possibly the heat transfer high enough, such that the liquid obtains the ambient temperature, i.e. $T^{(0)} = T_{\mathrm{a}}$.

In the case now of small heat transfer, $Bi = O(\varepsilon)$, the temperature profile across the sheet tends to be flat, i.e. $T^{(0)} = \theta(x, t)$ (as shown by 2.23). If in addition, we set the far-field temperature to be constant, say $T_{\mathrm{a}} = 0$, and the speed to be moderate such that $St = O(1)$, (2.24) reduces to

$$\partial_t \theta + \bar{u} \partial_x \theta = -St \, \frac{\theta}{h} \, . \tag{2.26}$$

This form of the thermal energy equation was first derived by Shah & Pearson (1972*a*) for fiber spinning — in which case h denotes the fiber radius — by solving (2.20) and (2.21) with the assumption $Bi \approx \varepsilon Pe = O(\varepsilon)$. Consequently, the temperature is found to be uniform across the thickness at leading order and the balance in (2.26) is found at next order. Equation (2.26) thus corresponds to the one-dimensional assumption for the temperature field, which is valid rigorously in the limited range of $St = O(1)$. It is worth noting that the first order balance (2.26) can be recovered from the leading order one (2.24) by taking the limit $Bi \to 0$. Therefore the parameter Bi in (2.24) appears as a measure of the departure from the one-dimensional assumption for the thermal energy equation. Indeed, our model (2.24) has been written with no restriction on neither Bi nor Pe, which should allow us to explore the entire range of Stanton numbers. Nevertheless, we note that for very large Pe, inertial effects that we have neglected in the momentum equation could become non-negligible as shown by Shah & Pearson (1972*b*) for fiber spinning and Cao *et al.* (2005) for film casting.

2.3. *The average viscosity*

The momentum and thermal energy equations are linked via the viscosity $\eta(T)$. We shall base our model for viscosity variations on the assumptions that no freezing occurs and that the fluid viscosity obeys the Arrhenius equation for molecular kinetics. In dimensionless form, we have

$$\eta(T) = e^{\mu \, (1/T - 1)} \, , \tag{2.27}$$

where μ measures the thermal sensitivity of the viscosity. For (2.15), we need the average viscosity over the thickness, which is essentially non-algebraic in y for a parabolic temperature profile $T^{(0)}$ as defined in the previous section. To proceed analytically, we then have to make an additional assumption on the temperature field, namely that its variation across the sheet remains small compared to the variations along the sheet, i.e. $|T^{(0)} - \theta| \ll 1$. This step allows us to average (2.27) across the thickness and truncate the result at first order in $T^{(0)} - \theta$ to obtain

$$\hat{\eta}(\theta) \approx e^{\mu \, (1/\theta - 1)} \, . \tag{2.28}$$

2.4. *The far-field temperature*

Practical applications of stretching viscous sheets might involve heat transfer by convection and/or radiation, which we simulate by using a non-constant ambient temperature, which can mimic in turn an imposed heat flux distribution, namely $Bi\, T_{\mathrm{a}}(x)$ since the Biot number is constant. We follow here the same approach as used by Willien *et al.* (1988) for fiber spinning and assume the far-field temperature to decrease exponentially along the stretching direction,

$$T_{\mathrm{a}}(x) = e^{-b\,x} \,, \tag{2.29}$$

where b is a positive parameter. Note that $T_{\mathrm{a}}(0) = 1$, which sets the dimensional far-field temperature equal to the surface temperature T_0 at inlet. This is necessary to ensure $|T^{(0)} - \theta| \ll 1$ at the inlet, regardless of the possibility of large Bi. Note some authors (e.g. Shah & Pearson (1972*a*) or Gupta *et al.* (1996)) have instead assumed that the heat transfer coefficient depends on the fluid velocity and hence increases along the stretching direction. Nevertheless, this has a significant influence only for large draw ratios, i.e. in a small region of the parameter space, and we therefore chose to keep the heat transfer coefficient α constant for simplicity. In fact, we shall show below that for $St \gg 1$, the critical draw ratio is as small as in isothermal conditions ($St = 0$) and the dependence of α with u can safely be neglected (see §5).

3. Stability problem

Let us analyze the stability of our model by writing the variables as

$$\bar{u}(x, t) = u_{\mathrm{s}}(x) \left(1 + U(x)\, e^{\lambda t}\right) \,, \tag{3.1a}$$

$$h(x, t) = h_{\mathrm{s}}(x) \left(1 + H(x)\, e^{\lambda t}\right) \,, \tag{3.1b}$$

$$\theta(x, t) = \theta_{\mathrm{s}}(x) \left(1 + \Theta(x)\, e^{\lambda t}\right) \,, \tag{3.1c}$$

$$f(t) = f_{\mathrm{s}} \left(1 + F\, e^{\lambda t}\right) \,, \tag{3.1d}$$

where the subscript 's' identifies the stationary solutions; U, H, Θ and F represent the perturbations (only the three first are complex) and λ is the eigenvalue. This approach to stability is common when analyzing viscous sheets (see e.g. Yeow (1974)). The system of equations to be solved can thus be recast into a set of ODEs for the base state and the perturbations.

3.1. *The base state*

Setting $\partial_t h = 0$ in (2.11), together with the boundary condition (2.16), leads to

$$h_{\mathrm{s}} = \frac{1}{u_{\mathrm{s}}} \,, \tag{3.2}$$

while the stress and temperature equations (2.15–2.24) for the base state are

$$u_{\mathrm{s}}' = \frac{f_{\mathrm{s}} u_{\mathrm{s}}}{\hat{\eta}(\theta_{\mathrm{s}})} \,, \tag{3.3a}$$

$$\theta_{\mathrm{s}}' = -St \frac{\theta_{\mathrm{s}} - T_{\mathrm{a}}}{1 + \frac{Bi}{6} h_{\mathrm{s}}} \,, \tag{3.3b}$$

where the prime denotes the x-derivative. These ODEs are to be solved with $u_{\mathrm{s}}(0) = \theta_{\mathrm{s}}(0) = 1$. Notice that if we neglect the thickness variation of the temperature (by setting

$Bi \to 0$), the base-state temperature, using (2.29), becomes

$$\theta_s(x) = \frac{b\,e^{-St\,x} - St\,e^{-b\,x}}{b - St} ,$$

which reduces to $\theta_s = e^{-St\,x}$ for $T_a = 0$, to $\theta_s = 1$ for $St = 0$ and to $\theta_s = T_a$ for $St \to \infty$.

3.2. *The perturbation equations*

Substituting (3.1) into (2.11), (2.15) and (2.24), while using the stationary solutions (3.2-3.3) for simplifications, yields three coupled ODEs

$$H' = -U' - \lambda h_s H , \tag{3.4a}$$

$$U' = \frac{f_s}{\hat{\eta}(\theta_s)} \left(F - U - H + \mu \frac{\Theta}{\theta_s} \right) , \tag{3.4b}$$

$$\Theta' = -\lambda h_s \Theta - \frac{St}{\theta_s(1 + \frac{Bi}{6}h_s)} \left[T_a\Theta - (\theta_s - T_a)\left(U + \frac{1 + \frac{Bi}{3}h_s}{1 + \frac{Bi}{6}h_s}\, H \right) \right] , \tag{3.4c}$$

which are to be solved with $H(0) = U(0) = U(1) = \Theta(0) = 0$. The amplitude F remains undetermined since the eigenvalue problem (3.4) is linear and homogeneous. This feature means the other amplitudes should be interpreted relative to F. In the following, we set $F = 0.1$.

4. Neutral stability

We focus in this work on the neutral stability of the system that separates stable and unstable regions in the parameter space formed by $Dr, St, Bi, \mu, T_a(x)$ and b. Thus we find solutions to the coupled system of ODEs (3.3–3.4), considering only the first mode of instability, i.e. the largest eigenvalue, when its real part is zero, namely $\lambda_R = \Re(\lambda) = 0$. Solutions to the problem have been sought by continuation using the software AUTO-07P (Doedel *et al.* 1997). As a starting point we used the analytical solution found by Renardy (2006) for isothermal conditions ($St = 0$) that belongs to the neutral stability curve with $\lambda_I = 14.01$ and $f_s = 3.006$, which corresponds to the classical result for the critical draw ratio $Dr_c = 20.218$, first obtained by Kase *et al.* (1966); Pearson & Matovich (1969); Gelder (1971)† for fiber spinning and by Yeow (1974) for film casting.

Neutral curves giving the critical draw ratio Dr_c, the frequency λ_I and the base-state tension f_s, versus the Stanton number St are plotted in figure 2 for $Bi = 6$, $b = 1$ and four different sensitivities μ of the viscosity with temperature. A maximum occurs at $St = O(1)$ and corresponds to the largest critical draw ratio, denoted 'S'. On the left of this maximum, the critical draw ratio increases with St, indicating a stabilizing effect of the heat transfer. This region will be referred hereafter to the advection-dominated regime, denoted 'A'. On the right of the maximum, the stability region decreases with increasing the Stanton number. This region will be referred hereafter to the transfer-dominated regime, denoted 'T'. In the limit of very large St, the critical draw ratio Dr_c can even lie below 20.218, which is unusual, at least for Newtonian liquids: $Dr_c < 20.218$ has indeed been reported for viscoelastic fluids (e.g. Smith & Stolle (2003)).

As shown in figure 2, the frequency λ_I and the tension f_s follow the same trend as

† Kase *et al.* (1966) and Pearson & Matovich (1969) showed independently that the isothermal fiber-spinning process has unstable normal modes, or resonances, at certain operating conditions in terms of draw ratio and forcing frequency, of which the lowest is for $Dr = 20.218$. Gelder (1971) determined that additionally to these resonances, the process is linearly unstable in the classical sense (i.e. temporal instability) for any draw ratio greater than 20.218.
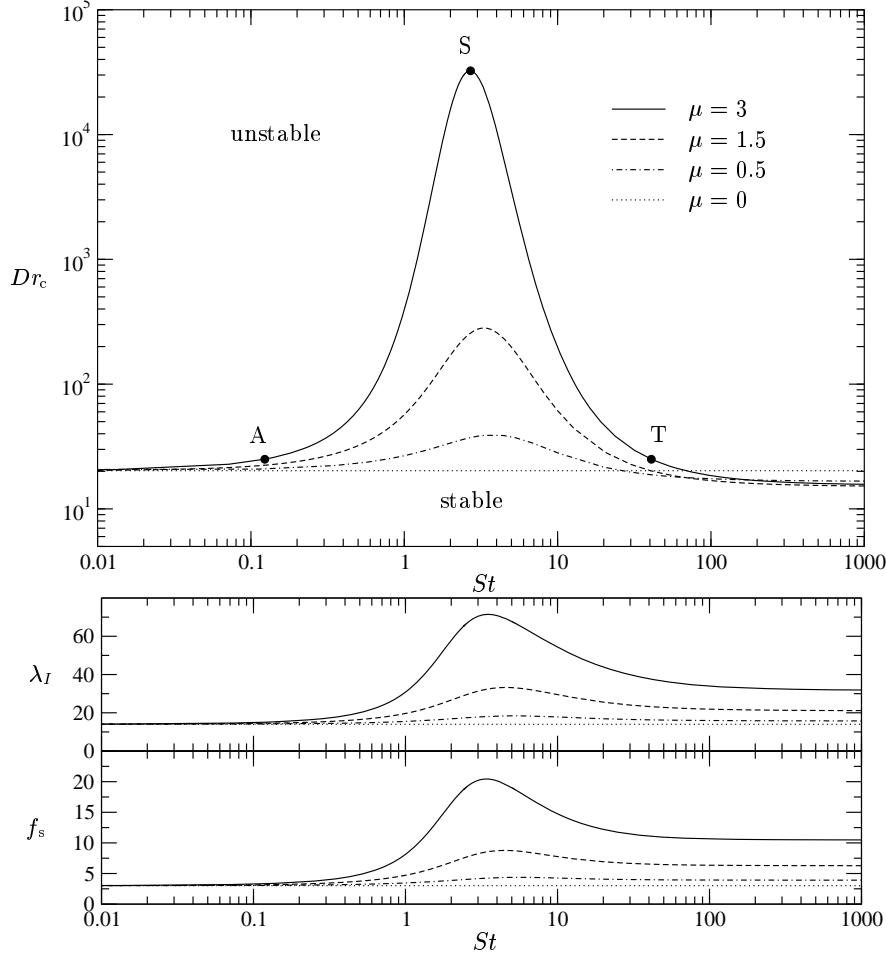
FIGURE 2. Neutral stability curves for $Bi/6 = b = 1$ and for different values of μ. Filled circles indicate solutions lying in the different regime of cooling: (A) Advection-dominated regime, (T) Transfer-dominated regime, (S) Largest critical draw ratio regime.

for Dr_c, except in the limit of very large St where their values are significantly larger than in isothermal conditions. This result means that a sheet with increasing viscosity along its stretching direction has a smaller period $P = 2\pi/\lambda_I$ of draw resonance than for a constant viscosity. Furthermore, except for this limit that will be analyzed in §5, increasing μ always stabilizes the system, as is observed commonly in fiber spinning and film casting.

Next, we want to compare our model that assumes a parabolic temperature profile across the sheet with the one-dimensional model assuming a constant temperature profile. The one-dimensional model is recovered simply by setting $Bi \to 0$ in (2.24). The neutral stability curves for $\mu = 3$ are plotted in figure 3(a), which shows that temperature variations across the sheet are stabilizing. Though this effect is small, it is obviously more pronounced as the Stanton number increases, i.e. in the region of large heat transfer ($St \geq 1$). Of course, temperature variations across the sheet should vanish in the limit of $St \to \infty$, for which the liquid temperature is everywhere identical to the ambient temperature T_a.
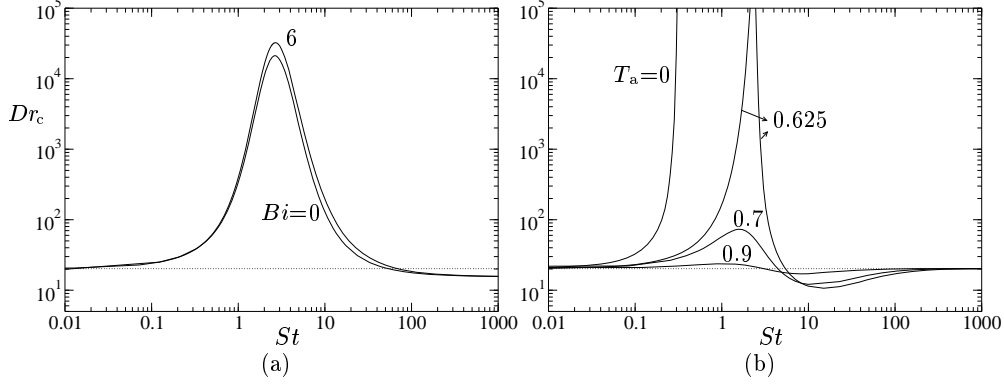
FIGURE 3. Neutral stability curve for $\mu = 3$. (a) Influence of the Biot number with $T_a = e^{-x}$, i.e. $b = 1$. (b) Influence of constant ambient temperatures T_a with $Bi \to 0$.

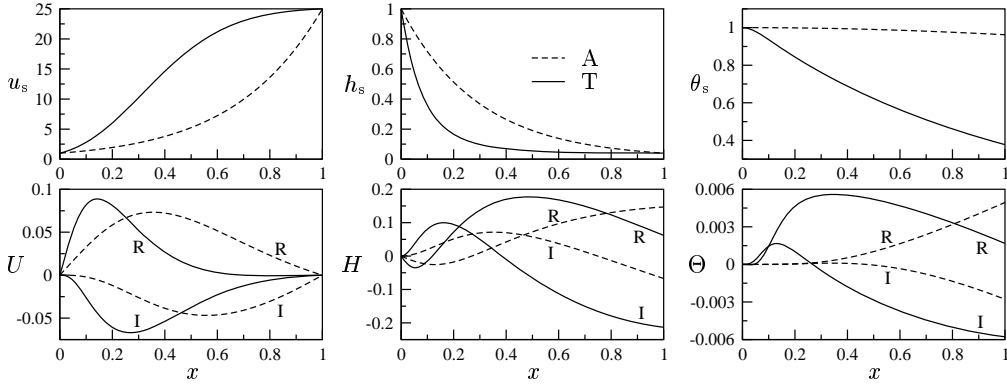FIGURE 4. Solutions to the eigenvalue problem (3.3–3.4) at criticality for $Dr_c = 25$ and $\mu = 3$, as identified in figure 2: (A) $St = 0.123$ (dashed lines) and (T) $St = 40.92$ (solid lines). The base-state solutions are above and the complex-valued perturbations below, with 'R' their real parts and 'I' their imaginary parts.

Figure 3(b) also shows the consequences of setting the ambient temperature to a constant. For $T_a = 0$ and $Bi \to 0$, (2.24) reduces to (2.26) as studied by Shah & Pearson (1972a) for fiber spinning. As found by these authors, the critical draw ratio rises abruptly as St increases, still in the region $St \ll 1$, leaving on the right of the neutral curve a large region of unconditional stability. However, the divergence of the neutral curve for $T_a = 0$ should only be attributed to the concomitant divergence of the viscosity as the fluid temperature approaches T_a, i.e. $\theta \to 0$ (see equation 2.28), when the Stanton number is increased. Figure 3(b) then shows that there is a range of finite values for T_a for which the neutral curves can be computed numerically up to large values of St, where they in turn all converge to the isothermal critical draw ratio $Dr_c = 20.218$: in the limit of infinite heat transfer coefficient, and for constant ambient temperature, the system exactly recover its isothermal state.

We next examine typical solutions for the steady-state and amplitudes of the perturbations. The results are plotted in figure 4 and correspond to the two different regions of the neutral stability curve for $\mu = 3$ in figure 2. In the region $St \ll 1$, the solution 'A' (dashed lines) in figure 4 shows a gentle temperature decrease along the stretching direction, hence the viscosity at take-up is only 12% larger than the inlet viscosity, so

that the stretched profiles (u_s, h_s) resemble those for isothermal stretching. Likewise, the corresponding amplitudes of the perturbations have no significant differences from the isothermal case. On the contrary, in the region of $St \gg 1$, the solutions (solid lines) show a different behavior, which is determined mainly by the strong decrease of the temperature θ_s that makes the viscosity at take-up about 140 times the inlet value. Most of the stretching thus occurs in the region of low viscosity as shown from the solutions for h_s and u_s in figure 4. The amplitudes of the perturbations are also distributed differently than those for isothermal conditions. The most significant difference is the real part of the velocity perturbation U (thick line), which reaches its maximum in the first-half of the film where the viscosity is the lowest, and decreases rapidly to zero in the second half. Though less obvious, this behavior is also the fate of the thickness perturbation, keeping in mind from (3.1) that the real perturbation is the product of H with the base state h_s, which is a minimum in the second half of the film.

Finally, in terms of the cooling process, and based on the definition of the Stanton number (2.25), we can summarize our observations as follows: (i) The region of $St \ll 1$ corresponds to an *advection-dominated* cooling for which an increase of the heat transfer coefficient stabilizes the system with respect to the draw resonance instability. These conditions are the usual situations found in industry for film casting and fiber spinning, where the system is found to be stable for draw ratios as large as $Dr = O(10^5)$. Typical Stanton numbers are smaller than unity, $St < 1$, and correspond to 'fast' flows, $Pe = O(100)$, and large film parameter, $\varepsilon = O(10^{-1})$. Note the heat transfer coefficient in this regime can still be very high, i.e. $Bi = O(1)$. (ii) The region of $St \gg 1$ corresponds to a *transfer-dominated* cooling, which, in contrast, is destabilized by an increase of the heat transfer coefficient. Practical examples would correspond to 'slow' flows, $Pe = O(10)$, and small film parameter, $\varepsilon = O(10^{-3})$, together with a large heat transfer coefficient. Typical processes that meet such conditions are found in the glass sheet industry where the Stanton number is commonly of $O(100)$.

5. Prescribed temperature limit

As mentioned in §2.2, in the limit of $St \to \infty$, the temperature of the sheet obtains the prescribed temperature of the ambient, i.e. $\theta_s = T_a = e^{-b\,x}$. If for the sake of simplicity, we further assume that the far-field temperature slightly decreases along the stretching direction, i.e. $b \ll 1$, then the temperature can be written as $\theta_s \approx 1 - b\,x$, which once substituted in (2.28) yields $\hat{\eta} \approx e^{\mu b\,x}$. Consequently, the viscosity is a prescribed function of position that only depends on the product μb and the stability problem can then be solved independently of the temperature equation and with μb as the only free parameter.

Neutral stability curves and solutions for this case are plotted in figure 5. For an exponential increase of the viscosity along the stretching axis, the results show that the critical draw ratio can be significantly below 20.218. However, as μb increases, the neutral curve saturates at $Dr_c \approx 16.5$, while the frequency of the instability increases quasi-linearly. Solution 'c' in figure 5 corresponds to a sheet whose viscosity at take-up is $e^{10} \approx 22000$ times the inlet viscosity. Such a large difference is common in the processing of highly viscous sheets.

Because the viscosity is an explicit function of position, $\hat{\eta}(x)$, there is an analytical solution for the base state,

$$u_s(x) = e^{f_s \int_0^x \frac{\mathrm{d}x'}{\hat{\eta}(x')}} \qquad \text{with} \quad f_s = \frac{\ln Dr}{\int_0^1 \frac{\mathrm{d}x}{\hat{\eta}(x)}} , \tag{5.1}$$
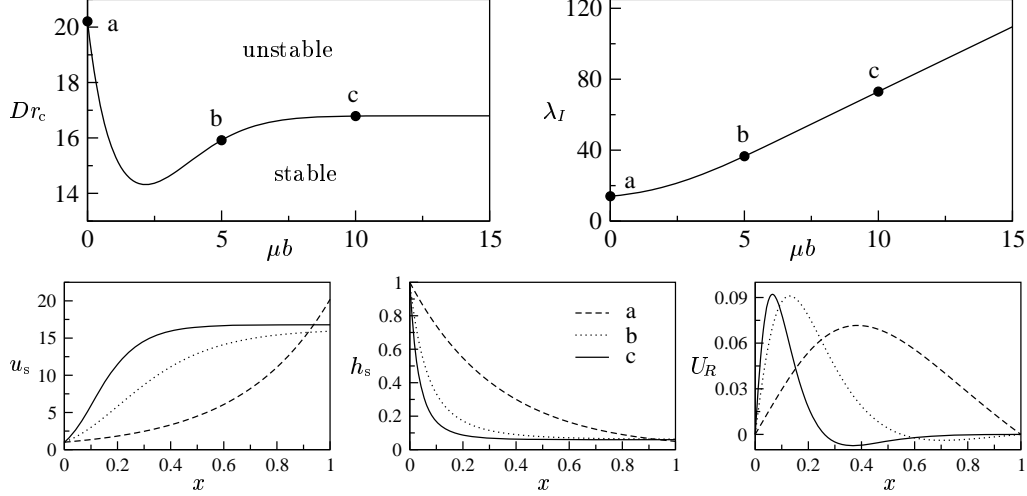
FIGURE 5. (Top) Neutral stability curves for Dr_c and λ_I in the 'prescribed temperature' limit. (Bottom) Typical solutions relative to μb.

and consequently the residence time τ_L of the fluid from the inlet to the take-up is

$$\tau_L = \int_0^1 \frac{\mathrm{d}x}{u_s} \ . \tag{5.2}$$

Since $h_s = 1/u_s$, it is straightforward to observe from figure 5 that the residence time decreases as the viscosity contrast μb increases; the liquid obtains a velocity close to the take-up speed in a shorter distance. For instance, the solution 'a' ($\mu b = 0$) in figure 5 corresponds to $\tau_L = 0.32$, while solution 'c' ($\mu b = 10$) corresponds to $\tau_L = 0.1$, which yields a factor three between the two residence times. According to the criterion proposed by Hyun (1978) and discussed in §6, a decrease of the residence time should be stabilizing, and this is the usual effect observed in the advection-dominated region. But as we have found in this study, this criterion is valid only if the period of draw resonance, denoted $P = 2\pi/\lambda_I$, remains unchanged as compared to the isothermal conditions. From figure 5, we rather see the frequency λ_I to be about three times larger for $\mu b = 10$ than for a constant viscosity ($\mu b = 0$). We conjecture here that this strong frequency increase of the draw resonance is related to the fact the stretching naturally occurs in the region close to the inlet where the viscosity is the lowest. In other words, these results are consistent with the idea that in the large Stanton number limit, a decrease of the *effective stretching length* is accompanied by an increase of the frequency of draw resonance.

6. Mechanism of draw resonance

Based on observations we have made so far, we propose in this section a scenario that simultaneously explains the stabilizing mechanism of draw resonance due to cooling, enhanced for increasing μ, and the destabilizing effect of strong viscosity variations along the stretching axis in the prescribed temperature limit. We first describe the mechanism of draw resonance in isothermal conditions and then propose a mechanism for non-isothermal conditions.

6.1. *Isothermal conditions: $St = 0$ (i.e. $\hat{\eta} = 1$)*

Draw resonance, in principle, can be seen as a resonance mechanism between a perturbation of the flow rate $q = \bar{u}h$, which evolves with time and position, and a perturbation of the film tension f, which only evolves in time (see e.g. Hyun (1999)). The tension is spatially independent, which ensures the instantaneous transfer of information between the two extremities of the sheet and hence allows for sustained oscillations of the thickness h around the centerline. Indeed, because at the take-up position, the speed Dr is fixed, (2.15) shows that the tension f is proportional to $h(1,t)$, or equivalently to the flow rate $Dr\,h(1,t)$. Next, because h is fixed at the inlet position (i.e. $\partial_t h\big|_0 = 0$), the continuity equation (2.11), using (2.15) and the boundary conditions, has the form†

$$\partial_x h\big|_0 = -f(t) . \tag{6.1}$$

This result shows in turn that a positive perturbation of the tension, say for f_{max}, induces a negative variation of the thickness right after the inlet, hence a negative variation of the flow rate (and vice-versa for f_{min}). As time evolves, this negative thickness variation reaches the take-up position, which constrains the force to decrease, inducing instantaneously an increase of the thickness variation at the inlet, again through (6.1). This cyclic mechanism was first outlined by Hyun (1978), who also proposed an approximate criterion for the onset of draw resonance that involves the comparison of two characteristic times in the system: the *unity-throughput time* t_L, which is the time for a wave of constant flow rate $q = 1$, also named a 'unity-throughput wave', to travel the system from the inlet to the take-up (see also appendix A) and the *residence time* τ_L, namely the time for the fluid to travel the system. Hyun (1978) established therefore that for the draw resonance instability to occur, a full cycle of throughput waves, a 'positive' $(\mathrm{d}f/\mathrm{d}t > 0)$ and a 'negative' $(\mathrm{d}f/\mathrm{d}t < 0)$ one, should travel through the system in a time smaller than the residence time. This criterion is based on the fact that the mass of fluid that enters the system at a constant rate (i.e. constant 'throughput') must leave the system in a fixed amount in every cycle of draw resonance.

In fact, as observed by Kim *et al.* (1996) from time-dependent simulations, the exact criterion should also account for a 'time delay', denoted Δt, between the tension that does not depend on position and the flow rate at take-up $q(1,t)$ (see also appendix B). This result follows because every half of a period, the vanishing of a perturbation of the tension f precedes by time Δt the moment at which a unity-throughput wave has reached the take-up. Therefore, for the instability to occur, i.e. for $Dr > Dr_{\mathrm{c}}$,

$$2t_L + \Delta t < \tau_L . \tag{6.2}$$

The important observation made by Hyun (1978), which is useful for understanding the mechanism underlying the draw resonance instability, is that during a full cycle of draw resonance, two unity-throughput waves travel the system, one triggered at f_{max} and the other one at f_{min}. A 'negative' (respectively, 'positive') wave is thus concomitant with a decrease (respectively, increase) of the axial tension. Figure 6 shows the time evolution of the local flow rate $q(x,t) = \bar{u}h$, as reconstructed from the solutions of the linear stability analysis. It shows half a cycle and illustrates with circles the traveling of the 'negative' unity-throughput wave. Because we focus on the linear response of the system, the picture is symmetric for the second half of the cycle: at time $t = P/2$, when the tension has reached its minimum, the 'positive' unity-throughput wave will start to travel during the same time t_L. It clearly appears from figure 6 that the only constant-flow-rate wave that travels over the entire domain is the one corresponding to $q = 1$. It

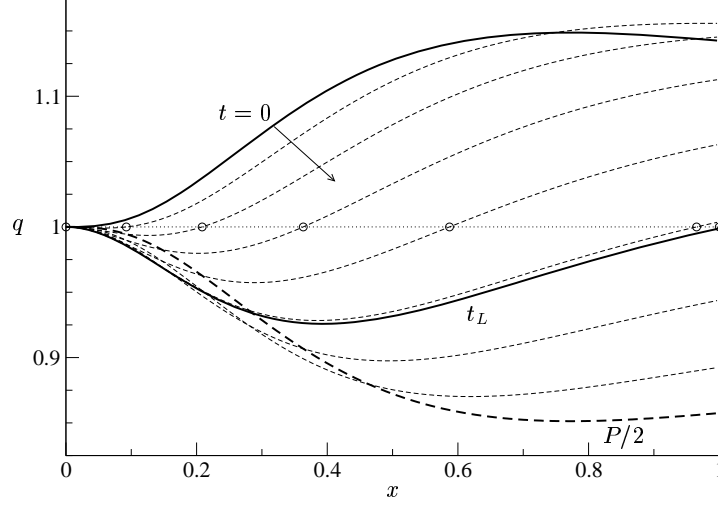† Note that (6.1) is always true, even in non-isothermal conditions.

FIGURE 6. Time evolution of the flow rate q at criticality ($Dr_c = 20.218$) for isothermal conditions ($St = 0$): the results start at $t = 0$ and are at intervals of $P/16$ (dashed lines) until half a period $P/2$, with $P = 0.448$. Circles represent the unity-throughput wave for $q = 1$ that starts at $x = 0$ at $t = 0$ and ends at $x = 1$ after a time $t_L = 0.142$.

also shows that the flow rate averaged over the domain will be as deficient as in excess, compared to the unity base-state flow rate, within one period of draw resonance. In fact, the perturbation equation (3.4b) integrated along the sheet leads to

$$ F = \frac{\int_0^1 \frac{Q+\Gamma}{\eta_s}\,\mathrm{d}x}{\int_0^1 \frac{1}{\eta_s}\,\mathrm{d}x} \ , \tag{6.3} $$

where $Q = U + H$ is the perturbation of the flow rate, $\Gamma = -\mu\Theta/\theta$ is the perturbation of the viscosity and $\eta_s = \hat{\eta}(\theta_s)$. This relation demonstrates that in isothermal conditions, i.e. $\Gamma = 0$ and $\eta_s = 1$, the flow-rate perturbation averaged over the domain evolves exactly in phase with variations of the tension, i.e. $F = \int_0^1 Q\,\mathrm{d}x$. In contrast, in non-isothermal conditions, the weighted mean of $(Q + \Gamma)/\eta_s$ is in phase with the tension f. This result thus means that an increasing viscosity along the sheet will induce a phase shift between the tension perturbation and the response of the averaged flow rate. This feature turns out to be crucial in understanding the (de)stabilization of draw resonance due to cooling.

6.2. Non-isothermal conditions: $St \neq 0$

Like the tension, averaged quantities do not depend on x coordinate, but only depend on time. They can thus be directly related to $f(t)$, especially in terms of the phase shift, based on the principle that the tension dictates the mechanism of draw resonance. Consequently, we define $\langle X \rangle (t) = \int_0^1 X(x,t)\,\mathrm{d}x$ as the average of quantity X at a given time t. Also, we write $\varphi_{\langle X \rangle}$ for the phase shift of this averaged quantity relative to oscillations of f taken as a reference, i.e. $\varphi_f = 0$, and normalized with the period P of oscillations.

Figure 7 shows, as predicted by (6.3), that the averaged flow rate $\langle q \rangle$ is in phase with the tension in the region of $St \ll 1$, and is delayed for increasing Stanton numbers. In the 'stabilized regime' for $St = O(1)$, i.e. at the transition S on figure 2, the averaged temperature $\langle \theta \rangle$ is nearly in phase with $\langle q \rangle$. The explanation for the stabilizing effect of cooling in this region of the parameter space is thus as follows: a perturbative increase
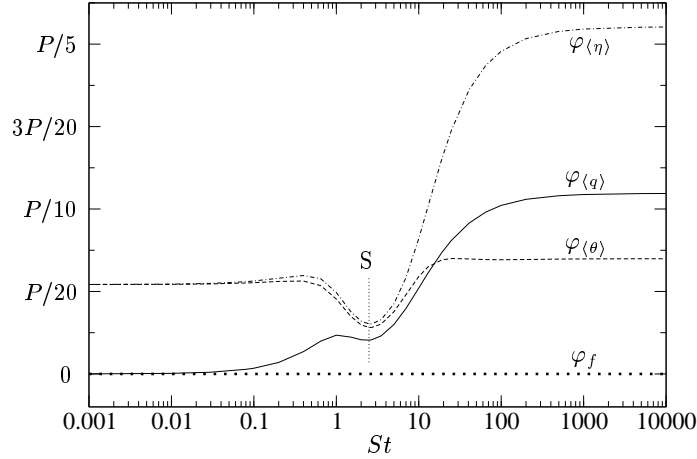
FIGURE 7. Phase shifts of different averaged quantities relative to the tension and normalized by the period P. The results correspond to the case $\mu = 3$ in figure 2. 'S' refers to the stabilized regime.

of the tension creates, after a small delay $\varphi_{\langle q \rangle}$, an increase of the average flow rate, which implies that in average, the liquid spends a little less time in the system and hence has a little less time to cool down. The averaged temperature $\langle \theta \rangle$ thus increases in response to an increase of the averaged flow rate. At the same time, $\varphi_{\langle \eta \rangle}$ and $\varphi_{\langle \theta \rangle}$ being nearly in phase in the stabilized regime, the averaged viscosity $\varphi_{\langle \eta \rangle}$ decreases accordingly, which in turn 'relaxes' the initial positive perturbation of the tension. This stabilization mechanism due to cooling is illustrated below for a positive perturbation of the tension,

$$\text{Perturbation} \;\Rightarrow\; f \nearrow \;\Rightarrow\; \langle q \rangle \nearrow \;\Rightarrow\; \langle \theta \rangle \nearrow \;\Rightarrow\; \langle \eta \rangle \searrow \;\Rightarrow\; f \searrow \;\Rightarrow\; \text{Damping}.$$
(6.4)

The same reasoning can be done for a negative perturbation, which is thus followed by an increase of the averaged viscosity, hence again a counter-action to the initial perturbation. This mechanism shows how the cooling process is stabilizing, or in other word why the critical draw ratio for draw resonance is much larger in the region of $St = O(1)$, as compared to isothermal conditions.

It is now easy to see that the above mechanism is most efficient in the region where the energy advected by the flow is comparable to the heat transfered to the surroundings, i.e. at the transition 'S' as labeled in figure 7. Indeed, in both limits of $St \to 0$ and $St \to \infty$, the temperature perturbation vanishes and the system behaves as if it was isothermal (see discussion in §2.2). The fact the amplitude of the temperature perturbation vanishes in those two limits can be seen from (3.4c) where

$$\text{if} \left\{ \begin{array}{l} St \to 0 \\ St \to \infty \end{array} \right. \;\Rightarrow\; \Theta \to 0 \quad \text{since} \left\{ \begin{array}{l} \Theta(0) = 0 \\ \theta_{\mathrm{s}} \to T_{\mathrm{a}} \end{array} \right. .$$
(6.5)

Note finally that for 'advection-dominated' cooling ($St \ll 1$), the averaged viscosity and temperature are exactly in phase, as for isothermal conditions. On the contrary for 'transfer-dominated' cooling ($St \gg 1$), the averaged viscosity is delayed relative to the averaged temperature and the phase shift with the tension is approaching a quarter of a period, which makes ineffective the stabilizing response of the averaged viscosity with tension perturbations.
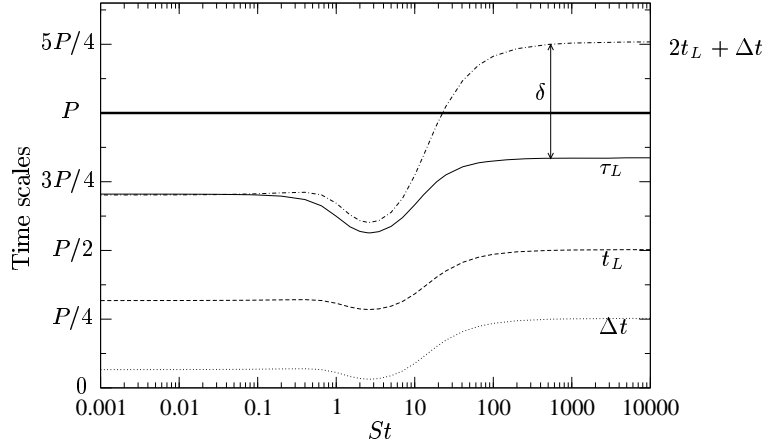
FIGURE 8. Characteristic times of the system normalized with the period P of draw resonance: τ_L the residence time, t_L the unity-throughput time, Δt the tension/thickness phase shift, and δ the viscous delay. The results correspond to the case $\mu = 3$ in figure 2.

7. Stability criterion in non-isothermal conditions

7.1. *Modification of Hyun's criterion*

In this section, we want to illustrate how Hyun's criterion is modified in non-isothermal conditions. To this aim, we have reported in figure 8 the different characteristic times of the system defined in the previous section (see also the appendices). We observe that the criterion (6.2) established for isothermal conditions is modified in non-isothermal conditions as follows,

$$2t_L + \Delta t < \tau_L + \delta \, , \tag{7.1}$$

where δ accounts for the delay induced by viscosity variations along the sheet. Note that δ is negligible in the 'advection-dominated' regime so that Hyun's criterion still applies in this region. On the contrary, δ becomes large (of the order of t_L) in the 'transfer-dominated' regime, indicating a dramatic effect of the viscosity variations on the stability properties. We also note by comparing figures 7 and 8 that δ and $\varphi_{\langle q \rangle}$ are closely correlated, in fact $\delta \approx 4\varphi_{\langle q \rangle}$. In order to illustrate this correlation, we show in figure 9 the time evolution of the flow rate for two different Stanton numbers corresponding to the most stable regime, $St = O(1)$, and to the 'prescribed-temperature' regime, $St \to \infty$. We notice that the flow rate in the first third of the domain in figure 9(a) behaves similarly to the isothermal case in the entire domain (see figure 6) — in the other two thirds, the flow rate is spatially constant and varies only with time. The critical draw ratio is extremely high in this case and the velocity in the constant-flow-rate region is so high that the residence time is negligible as compared to the time spent by the fluid in the first third of the domain. Consequently, the 'effective stretching' length is shortened by a factor 3, which is in favor of stability, and the 'effective draw ratio' is reduced to about $Dr^{2/3}$. We also observe that the unity-throughput wave accelerates strongly along x in figure 9(a) for the reason given above, while it decelerates in the limit $St \to \infty$ (figure 9(b)) due to the increase of the viscosity along the stretching direction. This effect is precisely measured by the time shift δ, however this parameter cannot be predicted from the linear theory. We shall therefore use instead the refined criterion of Kim *et al.* (1996) as shown below.
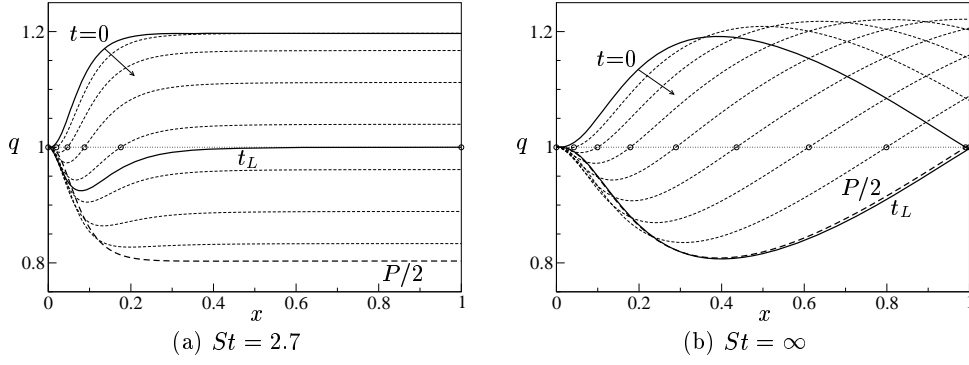
(a) $St = 2.7$ (b) $St = \infty$

FIGURE 9. Time evolution of the flow rate q at criticality, for two different Stanton numbers St and for $Bi/6 = b = 1$ and $\mu = 3$. Same legend as for figure 6 with (a) $Dr_{\rm c} = 32372$, $t_L = 0.026$, $P = 0.092$ and (b) $Dr_{\rm c} = 15.5$, $t_L = 0.1$, $P = 0.198$.

7.2. *Universality of Kim's criterion*

We gave in the Introduction the refined criterion (1.1) obtained by Kim *et al.* (1996) using traveling times of both unity-throughput waves t_L and extremum-thickness waves ϑ_L. In fact, Jung *et al.* (1999) have shown from time-dependent simulations the equivalence $\vartheta = P/2 + \Delta t$ such that (1.1) can be rewritten as

$$t_L \leq \frac{P}{4} + \Delta T \qquad \text{for} \qquad Dr \geq Dr_{\rm c} \,, \tag{7.2}$$

where all quantities involved have already been determined in the previous section (see also the appendices). While the equality at threshold can easily be verified by looking at figure 8, we have also verified (not shown) that the inequality in (7.2) applies well for the entire range of Stanton numbers. Consequently, the universality of criterion 7.2 is confirmed since it not only applies to viscoelastic film casting but also here to non-isothermal film casting.

8. Concluding remarks

We have investigated the stability of a stretching viscous sheet for the entire range of Stanton numbers and have identified two regimes: one dominated by advection of energy as is commonly found in the literature for fiber spinning and film casting whose process parameters typically correspond to $St \lesssim 1$, and one dominated by heat transfer to the environment as encountered for instance in the glass sheet industry whose process parameters typically correspond to $St \gg 1$. While heat transfer has a stabilizing effect in the first regime, it has a destabilizing effect in the second one where the liquid sheet approaches the imposed temperature of the surrounding as St increases. To some extent, this regime can be associated with a cooling dominated by radiative heat transfer rather than by convective heat transfer, as is the case for manufacturing glass sheets. This conclusion is supported by the work by Willien *et al.* (1988) who found in fiber spinning that radiative heat transfer can be destabilizing, which is opposite to the response for the case where convective heat transfer is dominant.

We also propose a mechanism that qualitatively explains the stabilizing effect due to cooling, which is most efficient in the region where the energy advected by the flow and energy transfered to the ambient are comparable, i.e. for $St = O(1)$. In this region, the average viscosity is shown to act quasi-instantaneously against a perturbation of the

tension, as a consequence of an in-phase variation of the axial-averaged flow rate and axial-averaged temperature.

In the limit of $St \to \infty$, the temperature of the sheet is shown to be prescribed by the temperature of the ambient environment, which leads to a useful simplification where the viscosity is a prescribed function of the coordinates. Nevertheless, we have to remember that at finite St, the temperature field always stabilizes the system compared to the infinite St limit. This limit represents then the 'worst case', where the critical draw ratio can be below its value for isothermal conditions when increasing the temperature sensitivity of the viscosity, at least in the case of symmetrical thermal boundary conditions. In the case of non-symmetrical thermal boundary conditions, the present model would also account for viscosity variation in the transverse direction. This subject is one for future study.

Appendix A. Unity-throughput time

The continuity equation (2.11) can be written in the form of a kinematic wave for a fluid element h,

$$\partial_t h + u\partial_x h = -h\partial_x u \,, \tag{A 1}$$

where u is the phase speed and the right-hand side represents the global attenuation due to the effective tension (since $h\partial_x u = f/\hat{\eta}$ from 2.15). Likewise and as in Kim *et al.* (1996), we can write the kinematic equation for a wave of conserved flow rate $q = uh$ as follows,

$$\partial_t q + c\,\partial_x q = 0 \,, \tag{A 2}$$

where $c = c(x)$ is the phase speed of such a wave. Linearizing (A 2) with $q = 1 + Q\,e^{\lambda t}$ leads to

$$Q' = -\frac{\lambda}{c}\,Q \,, \tag{A 3}$$

which can be identified with (3.4a), provided $Q = H + U$, to yield

$$c = \frac{Q}{h_{\mathrm{s}}\,H} \,. \tag{A 4}$$

Now the only constant-flow-rate wave that travels the entire system is the one corresponding to $q = 1$, referred to as the *unity-throughput wave* (Kim *et al.* 1996). The time this wave will travel the system is therefore the *unity-throughput time*, obtained as

$$t_L = \int_0^1 \Re\left(\frac{1}{c}\right)\,\mathrm{d}x = \int_0^1 h_{\mathrm{s}}\frac{(H_R Q_R + H_I Q_I)}{(Q_R^2 + Q_I^2)}\,\mathrm{d}x \,. \tag{A 5}$$

Appendix B. Phase shifts

In draw resonance, because of the boundary conditions, the tension and the thickness variations are in phase inversion right after the inlet, as shown by (6.1), while they are close but not in phase at the take-up. Indeed, unless $\partial_x u|_1$ is in phase with $h(1,t)$, and based on (2.15), there is no reason for $h(1,t)$ to be exactly in phase with f. On the basis that f leads h, the phase shift between the two can be calculated by applying a

trigonometric factorization as follows,

$$H_R \cos(\lambda_I t) - H_I \sin(\lambda_I t) = H_R \frac{\cos(\lambda_I t - \phi)}{\cos(\phi)} \qquad \text{with} \qquad \tan\phi = -\frac{H_I}{H_R} \; , \qquad \text{(B 1)}$$

such that the phase shift Δt at the take-up between $h(1, t)$ (also $\propto q(1, t)$) and f has the form

$$\Delta t = -\frac{1}{\lambda_I} \arctan\left(\frac{H_I(1)}{H_R(1)}\right) \; . \qquad \text{(B 2)}$$

Likewise, the phase shift of any averaged quantity $\langle X \rangle$ is given as

$$\varphi_{\langle X \rangle} = -\frac{1}{\lambda_I} \arctan\left(\frac{\langle X_s X_I \rangle}{\langle X_s X_R \rangle}\right) \; . \qquad \text{(B 3)}$$

REFERENCES

BAROT, G. & RAO, I.J. 2004 Modeling the film casting process using a continuum model for crystallization in polymers. *Int. J. Nonlinear Mech.* **40**, 939.

BUCKMASTER, J.D., NACHMAN, A. & TING, L. 1975 The buckling and stretching of a viscida. *J. Fluid Mech.* **69**, 1–20.

CAO, F., KHAYAT, R.E. & PUSKAS, J.E. 2005 Effect of inertia and gravity on the draw resonance in high-speed film casting of Newtonian fluids. *Int. J. Solids Struct.* **42**, 5734–5757.

DEWYNNE, J.N., OCKENDON, J.R. & WILMOTT, P. 1992 A systematic derivation of the leading-order equations for extensional flows in slender geometries. *J. Fluid Mech.* **244**, 323–338.

DOEDEL, E.J., CHAMPNEYS, A., FAIRFRIEVE, T., KUZNETSOV, Y., SANDSTEDE, B. & WANG, X. 1997 Auto97 continuation and bifurcation software for ordinary differential equations. *Montreal Concordia University* Auto software is freely distributed on http://indy.cs.concordia.ca/auto/.

FISHER, R.J. & DENN, M.M. 1977 Mechanics of nonisothermal polymer melt spinning. *AIChE* **23**, 23–28.

FOREST, M. G., ZHOU, H. & WANG, Q. 2000 Thermotropic liquid crystalline polymer fibers. *SIAM J. Appl. Math.* **60**, 1177.

GELDER, D. 1971 The stability of fiber drawing processing. *Ind. Eng. Chem. Fundam.* **10**, 534–535.

GEYLING, F.T. & HOMSY, G.M. 1980 Extensional instabilities of glass fibre drawing process. *Glass Tech.* **21**, 95–102.

GUPTA, G.K., SCHULTZ, W.W., ARRUDA, E.M. & LU, X. 1996 Nonisothermal model of glass fiber drawing stability. *Rheol. Acta* **35**, 584–596.

HOWELL, P.D. 1996 Models for thin viscous sheets. *Euro. J. Appl. Math.* **7**, 321–343.

HYUN, J.C. 1978 Theory of draw resonance. *AIChE* **24**, 418–422.

HYUN, J.C. 1999 Draw resonance in polymer processing: a short chronology and a new approach. *Korean-Australia Rheol. J.* **11**, 279–285.

JUNG, H.W., CHOI, S.M., & HYUN, J.C. 1999 Approximate method for determining the stability of the film-casting process. *AIChE* **45**, 1157.

JUNG, H.W., SONG, H.-S. & HYUN, J.C. 2000 Approximate method for determining the stability of the film-casting process. *AIChE* **46**, 2106.

KASE, S., MATSUO, T. & YOSHIMOTO, Y. 1966 Theoretical analysis of melt spinning. Part 2: Surging phenomena in extrusion casting of plastic films. *Seni Kikai Gakkai Shi* **19**, T63.

KIM, B.M., HYUN, J.C., OH, J.S. & LEE, S.J 1996 Kinematic waves in the isothermal melt spinning of Newtonian fluids. *AIChE* **42**, 3164–3169.

LEE, J. S., JUNG, H. W. & HYUN, J. C. 2005 Simple indicator of draw resonance instability in melt spinning processes. *AIChE* **51**, 2869.

MINOSHIMA, W. & WHITE, J.L. 1983 Stability of continuous film extrusion processes. *Polym. Eng. Rev.* **2**, 211.

PEARSON, J.R.A. 1985 *Mechanics of Polymer Processing.* Elsevier Applied Science Publishers.

PEARSON, J.R.A. & MATOVICH, M.A. 1969 Spinning a molten threadline – Stability. *Ind. Eng. Chem. Fundam.* **8**, 605–609.

RENARDY, M. 2006 Draw resonance revisited. *SIAM J. Appl. Math.* **66**, 12611269.

SHAH, Y.T. & PEARSON, J.R.A. 1972*a* On the stability of nonisothermal fiber spinning. *Ind. Eng. Chem. Fundam.* **11**, 145–149.

SHAH, Y.T. & PEARSON, J.R.A. 1972*b* On the stability of nonisothermal fiber spinning – General case. *Ind. Eng. Chem. Fundam.* **11**, 150–153.

SHIN, D.M., LEE, J.S., KIM, J.M., JUNG, H.W. & HYUN, J.C. 2007 Transient and steady-state solutions of 2d viscoelastic nonisothermal simulation model of film casting process via finite element method. *J. Rheol.* **51**, 393–407.

SILAGY, D., DEMAY, Y. & AGASSANT, J.-F. 1996 Study of the stability of the film casting process. *Polym. Eng. Sci.* **36**, 2614–2625.

SMITH, S. & STOLLE, D. 2000 Nonisothermal two-dimensional film casting of a viscous polymer. *Polym. Eng. Sc.* **40**, 1870.

SMITH, S. & STOLLE, D. 2003 Numerical simulation of film casting using an updated Lagrangian finite element algorithm. *Polym. Eng. Sc.* **43**, 1105–1122.

SOLLOGOUB, C., DEMAY, Y. & AGASSANT, J.-F. 2006 Non-isothermal viscoelastic numerical model of the cast-film process. *J. Non-Newtonian Fluid Mech.* **138**, 76–86.

WILLIEN, J.-L., DEMAY, Y. & AGASSANT, J.-F. 1988 Stretching stability analysis of a Newtonian fluid: application to polymer spinning and glass drawing. *J. Theor. Appl. Mech.* **7**, 719–739.

WYLIE, J.J., HUANG, H. & MIURA, R. M. 2007 Thermal instability in drawing viscous threads. *J. Fluid Mech.* **570**, 1.

YEOW, Y.L. 1974 On the stability of extending films: a model for the film casting process. *J. Fluid Mech.* **66**, 613–622.

ZHENG, H., YU, W., ZHOU, C. & ZHANG, H. 2006 Three-dimensional simulation of the non-isothermal cast film process of polymer melts. *J. Polym. Res.* **13**, 433.